This is an open access article published under an ACS AuthorChoice License, which permits copying and redistribution of the article or any adaptations for non-commercial purposes.

ACS APPLIED MATERIALS & INTERFACES

Research Article

Cite This: ACS Appl. Mater. Interfaces 2018, 10, 25393−25400

www.acsami.org

Toward Tandem Solar Cells for Water Splitting Using Polymer Electrolytes

Ainhoa Cots,[†] Pedro Bonete,[†] David Sebastián,[‡,§] Vincenzo Baglio,[‡] Antonino S. Aricò,[‡] and Roberto Gómez*[,†]

[†]Departament de Química Física i Institut Universitari d'Electroquímica, Universitat d'Alacant, Apartat 99, E-03080 Alicante, Spain

[‡]Consiglio Nazionale delle Ricerche—Instituto di Tecnologie Avanzate per l'Energia "Nicola Giordano", CNR-ITAE, Via Salita Santa Lucia sopra Contesse 5, 98126 Messina, Italy

Supporting Information

ABSTRACT: Tandem photoelectrochemical cells, formed by two photoelectrodes with complementary light absorption, have been proposed to be a viable approach for obtaining clean hydrogen. This requires the development of new designs that allow for upscaling, which would be favored by the use of transparent polymer electrolyte membranes (PEMs) instead of conventional liquid electrolytes. This article focuses on the photoelectrochemical performance of a water-splitting tandem cell based on a phosphorus-modified α-Fe_2O_3 photoanode and on an iron-modified CuO photocathode, with the employment of an alkaline PEM. Such a photoelectrochemical cell works even in the absence of bias, although significant effort should be directed to the optimization of the photoelectrode/PEM interface. In addition, the results reveal that the employment of polymer electrolytes increases the stability of the device, especially in the case of the photocathode.

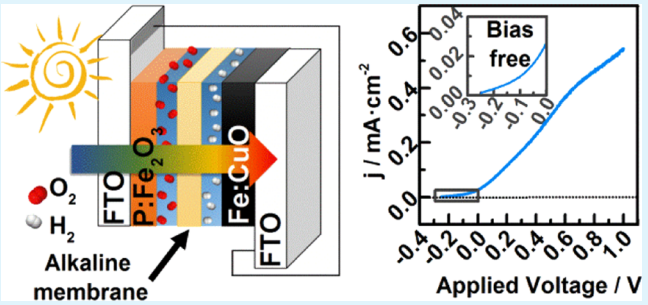

KEYWORDS: *bias-free water splitting, hematite, copper(II) oxide, photoelectrochemical cell, polymer electrolyte membrane*

INTRODUCTION

The growing use of fossil fuels due to the increasing global energy demand and the concomitant emission of greenhouse and pollutant gases to the atmosphere have motivated the scientific community to search for environmentally friendly alternative energy sources. In this regard, solar energy and, more concretely, photoelectrochemical (PEC) water splitting may play an important role in the future, being used for producing hydrogen as a carbon-free fuel. Tandem cells formed by two photoelectrodes with complementary light absorption are considered to be key devices for obtaining hydrogen in a carbon-free, renewable, and inexpensive way.[1−4]

Although a substantial effort has been done for the preparation and characterization of new electrode materials, the design of realistic devices that can be scaled up in a straightforward way has received little attention. In this respect, the use of a polymer electrolyte membrane (PEM) is of relevant interest to avoid internal recombination of photogenerated hydrogen and oxygen while allowing for appropriate ion transport. The use of a PEM allows for efficient gas separation, which is an important issue of electrolysis and photoelectrolysis systems.[5−7] Moreover, regarding the issue of photoelectrode stability in aqueous solutions, the employment of a PEM is a well-known alternative because no concentrated corrosive electrolytes are, in principle, necessary but just pure water can be sufficient.[7] PEM and ionomer dispersions are part of the advanced device and they help to maximize the overall performance of the photoelectrolysis system and to prevent corrosion, especially in the case of semiconductors with relatively narrow energy gap.[7]

Among the large number of semiconductor materials suggested as candidates for PEC water splitting, hematite has been widely employed as a photoanode because of its abundance, stability, low cost, and favorable band gap.[8,9] However, its use is limited because of the high recombination rate, low carrier mobility, and slow carrier transfer.[8,10−12] To overcome these limitations, several studies have focused on different strategies of modification,[13−17] the enhancement of electron mobility being one of them. Zhao et al. have demonstrated that a nonmetal such as phosphorus can be an excellent dopant to improve the PEC activity of hematite photoanodes.[18] On the other hand, cupric oxide is a promising candidate as a photocathode material because of its band gap, narrow enough to harvest a significant fraction of solar radiation. It presents low toxicity, low cost, and efficient light harvesting.[19−22] However, a major drawback for CuO to be used as an efficient photocathode in PEC water splitting is its instability in aqueous solution containing corrosive electro-

Received: April 26, 2018
Accepted: July 3, 2018
Published: July 19, 2018

Downloaded via UNIV DE ALICANTE on August 31, 2018 at 10:00:47 (UTC).
See https://pubs.acs.org/sharingguidelines for options on how to legitimately share published articles.

© 2018 American Chemical Society

DOI: 10.1021/acsami.8b06826
ACS Appl. Mater. Interfaces 2018, 10, 25393−25400

Scheme 1. Different Schemes of the Tandem Devices Studied[a]

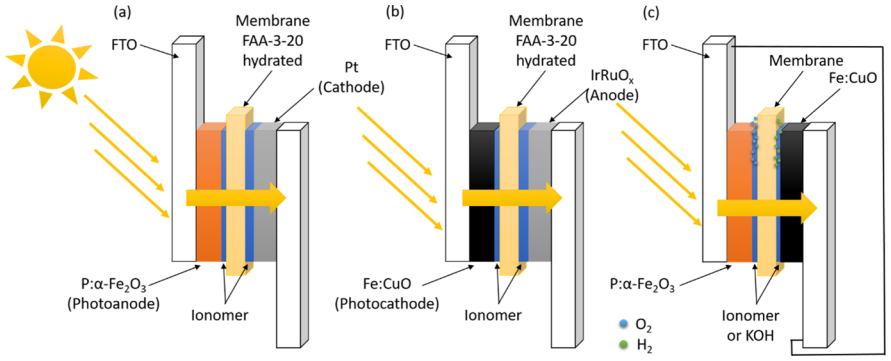

[a]In the three cases, the interface electrode−membrane is formed by either a droplet (15 μL) of the ionomer dispersion (different dilution levels) or 0.1 M KOH solution. The alkaline membrane FAA-3-20 is sandwiched between both photoelectrodes. The PEC cells studied are (a) formed by a photoanode P:α-Fe_2O_3 and a Pt dark electrode as a cathode, (b) formed by a photocathode Fe/CuO and an $IrRuO_x$ electrode as a dark anode, and finally (c) formed by a photoanode of P:α-Fe_2O_3 and a photocathode of Fe/CuO, being illuminated through the photoanode side.

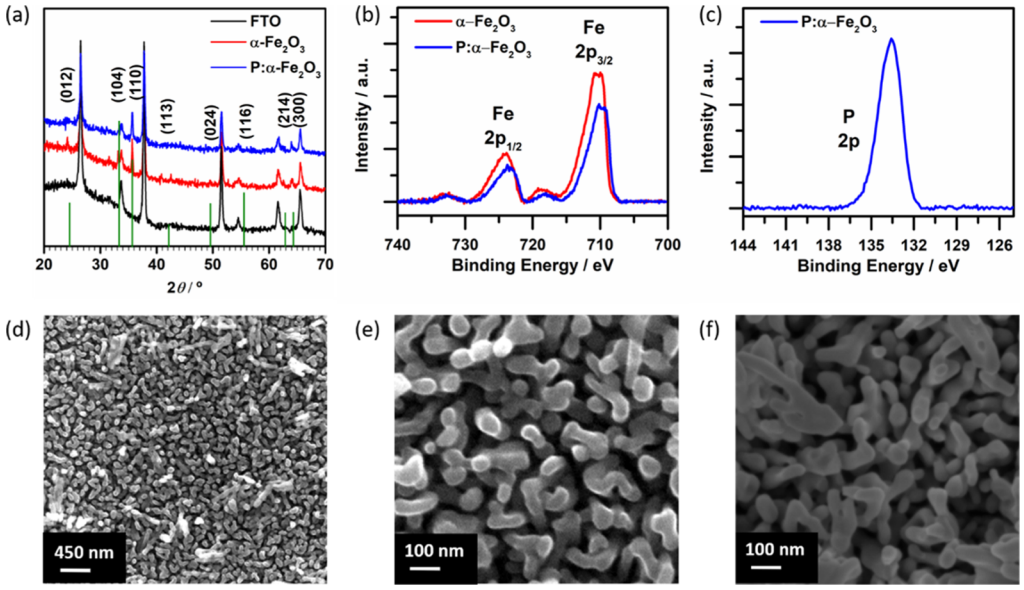

Figure 1. (a) X-ray diffractogram for pristine hematite (red) and hematite modified with phosphorus (blue). The hematite main reflections are labeled. The unlabeled peaks correspond to the conducting glass substrate (F/SnO_2). (b) Fe 2p XPS spectra for pristine hematite (red) and hematite modified with phosphorus (blue). (c) P 2p XPS spectrum for hematite modified with phosphorus. (d,e) SEM images of hematite modified with phosphorus by spray pyrolysis at different magnifications and (f) SEM image of pristine hematite.

lytes. Photocorrosion significantly decreases performance and shortens lifetime. Different strategies have been studied to increase the stability of CuO.[23−25] It is noteworthy that the employment of a thin metal-alloyed CuO layer on a pristine CuO thin film increases stability, although it decreases the resulting photocurrent.[25]

In this work, critical advances in the development of a tandem solar cell for water splitting using a transparent PEM are highlighted. The employed photoanode is based on hematite modified with phosphorus by spray pyrolysis (P:α-Fe_2O_3), whereas the photocathode is based on a CuO nanostructure modified with a $Cu_xFe_yO_z$ shell to increase the stability of cupric oxide (Fe/CuO).[26] The tested devices consist of an alkaline PEM (anion-exchange membrane polymer electrolyte) sandwiched between a P:α-Fe_2O_3 electrode working as a photoanode and an Fe/CuO electrode working as a photocathode. Either ultrathin films of deposited ionomer dispersions or small volumes (μL) of the electrolyte (0.1 M KOH) are used to improve the contact between electrodes and PEM (see Scheme 1).

RESULTS AND DISCUSSION

Both photoelectrodes, hematite modified with phosphorus and cupric oxide modified with iron, were characterized by means of X-ray diffraction (XRD), X-ray photoelectron spectroscopy (XPS), and scanning electron microscopy (SEM).

Figure 1 summarizes the characterization of the phosphorus-modified hematite photoanode. The XRD patterns confirm the presence of (110) oriented hematite in both pristine hematite and P:α-Fe_2O_3. From Figure 1b, the XPS spectra of Fe 2p are attributed completely to the Fe^{3+} oxidation state in both cases, pristine and P:α-Fe_2O_3. The P 2p XPS spectrum shown in Figure 1c exhibits the main peak centered at 133.5 eV, the characteristic peak of oxidized phosphorus species. It could be ascribed to P^{5+} atoms in PO_4^{3-} anions.[27,28] As observed from SEM images (Figure 1d,e), the hematite films modified with

DOI: 10.1021/acsami.8b06826
ACS Appl. Mater. Interfaces 2018, 10, 25393−25400

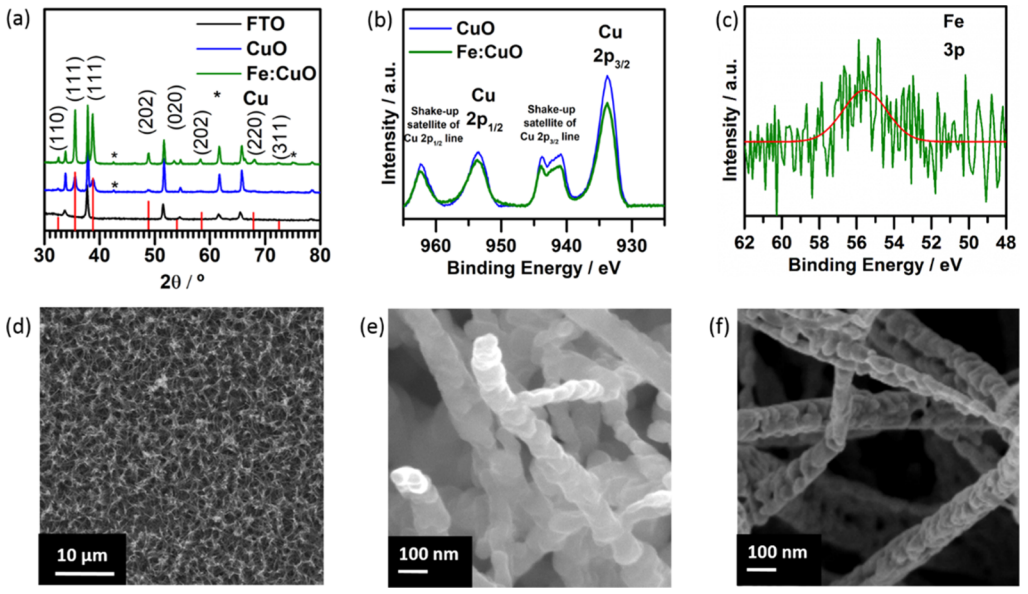

Figure 2. (a) X-ray diffractograms for copper oxide (blue) and copper oxide modified with iron (green). The CuO main reflections are labeled. The unlabeled peaks correspond to the conducting glass substrate (F/SnO_2), (b) Cu 2p XPS spectra for cupric oxide (blue) and cupric oxide modified with iron (green), (c) Fe 3p XPS spectra for copper oxide modified with iron, (d,e) SEM images at different magnifications of copper oxide modified with iron by means of drop-casting, and (f) SEM images of copper oxide.

phosphorus present a morphology of nanorods as pristine hematite (Figure 1f), although some of them seem to be coalescing.

Figure 2 shows the XRD, XPS, and SEM characterization of electrodes made of CuO and CuO modified with iron. The crystal phase of both samples can be readily indexed to the monoclinic structure. The four peaks obtained in the Cu 2p XPS spectra (Figure 2b) are clearly attributed to CuO, and the presence of iron in the film does not affect the oxidation state of copper.[29] In the case of Fe, we have chosen to show the Fe 3p spectrum as the Fe 2p region was overlapped by rather strong copper Auger peaks. The low amount of Fe dopant leads to a weak signal at 55.8 eV. It can be attributed to Fe^{3+} in an environment similar to that in hematite. The presence of Fe in the films was confirmed by energy-dispersive X-ray spectroscopy (Figure S1 in the Supporting Information). The films based on copper oxide modified with iron present the same morphology of nanowires as the pristine material. However, the diameter of these nanowires increases from around 70 nm in the case of cupric oxide to around 88 nm in the case of Fe/CuO; this fact is related to the formation of a $Fe_xCu_yO_z$ shell covering CuO and thus stabilizing it.

Once both electrode materials were characterized, the procedure for forming the interface between the photoelectrode and the ion-exchange membrane (20 μm thick, quaternary ammonium-based anionic membrane from Fumatech, i.e., Fumion Fumasep FAA-3-20)[7] by applying an ultrathin layer of an ionomer onto the semiconductor surface was studied. The ionomer dispersion formulation was the same as for the FAA-3-20 membrane. Both are characterized by the presence of fixed terminal quaternary ammonium groups counterbalanced by mobile hydroxyl (OH^-) ions. In the tandem concept, the PEM separator must be transparent in the range of wavelengths that are not absorbed by the higher energy gap semiconductor photoelectrode, first exposed to sunlight (P:α-Fe_2O_3 in the present case). Thus, the lower band gap semiconductor photoelectrode can absorb part of the transmitted light besides the diffuse light. Figure S2 effectively shows that the FAA-3-20 membrane is characterized by such requisite. Drop-casting was used as the ionomer deposition method and different dilution factors of the ionomer dispersion (FAA3) with isopropanol were tested (ranging from nondiluted to dispersion/isopropanol = 1:5). The deposited ionomer was dried to allow evaporation of the solvent before being hydrated with water.

Initially, a preliminary study employing only one photoelectrode and a dark electrode was carried out (see Scheme 1a,b). The response of the devices based on the photoelectrode P:α-Fe_2O (Scheme 1a) is shown in Figure 3. An electrochemical characterization comprising current−voltage curves recorded both in the dark and under illumination as well as electrochemical impedance spectra (EIS) obtained under illumination was undertaken as a function of the degree of dilution of the ionomer dispersion. For the P:α-Fe_2O_3 device, the maximum photoresponse was obtained for a diluted dispersion, a 1:4 dilution being adopted for further studies. Minimum polarization resistance was observed in this case (Figure 3c). The need for dilution could be linked to the fact that the hematite film presents a rather compact nanorod morphology making it difficult for the ionomer to penetrate in the nanostructure if dosed from a concentrated dispersion.

An analogous study was performed with a Fe/CuO photocathode interfaced to the alkaline membrane FAA-3-20 (see Figure 4 and Scheme 1b). In this case, the best (photo)response at lower potentials is reached with a nondiluted ionomer dispersion, whereas at intermediate potentials, a 1:2 dilution appears to be more effective (Figure 4b). The large photocurrent achieved with the nondiluted ionomer dispersion at negative potentials is probably related to the structure of the CuO electrode, more open than that of the hematite counterparts, allowing for the effective loading of larger amounts of the ionomer, thus providing a suitable extension of the interface between the semiconductor nanorods and the polymer electrolyte.

DOI: 10.1021/acsami.8b06826
ACS Appl. Mater. Interfaces 2018, 10, 25393−25400

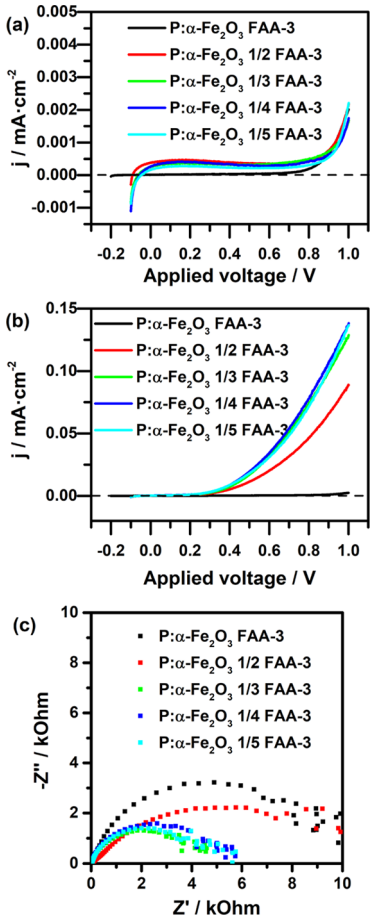

Figure 3. Current density−voltage curves obtained (a) in the dark and (b) under standard illumination (AM 1.5G, 100 mW·cm^{-2}) and (c) Nyquist plots collected at 1 V bias under standard illumination for the different cells studied using P/Fe_2O_3 as a photoanode and Pt as a cathode with different dilution levels of the ionomer dispersion.

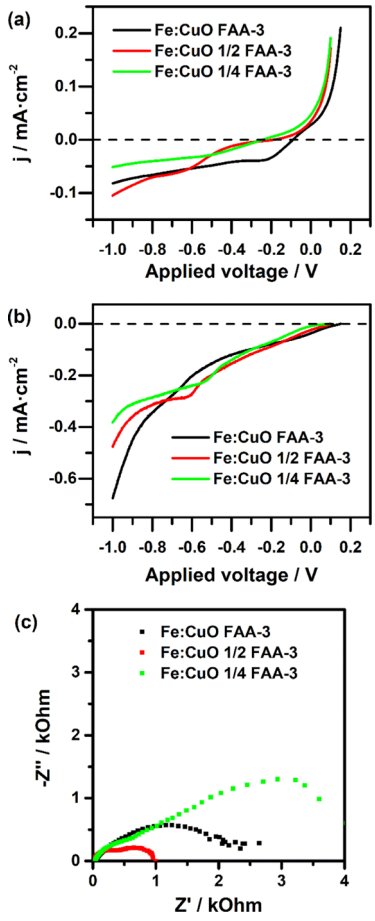

Figure 4. Current density−voltage curves obtained in (a) the dark and (b) under standard illumination (AM 1.5G, 100 mW·cm^{-2}) and (c) Nyquist plots collected at 1 V bias under standard illumination for the different cells studied using copper oxide modified with iron as a photocathode and iridium ruthenium oxide as an anode with different dilution levels of the ionomer dispersion.

Taking these results into account, the tandem cell configurations studied here are those depicted in Scheme 2. As observed, to improve the contact between the electrode and the PEM, the simple application of a droplet of a 0.1 M KOH aqueous solution on the electrode surface prior to its assembly with the PEM was attempted together with the above-mentioned application of the ionomer dispersion. A picture of the experimental device is shown in Figure S4.

Figure 5 shows the photocurrent density versus voltage obtained for the different tandem cells under standard illumination. As observed in Figure 5b, the tandem cells can work without the application of a bias, even if the photocurrent is still low under these conditions. More concretely, the tandem cell number 1 employing 0.1 M KOH between the two photoelectrodes and the membrane presents the maximum response for a bias-free device. For relatively large applied bias, the use of an ionomer in one or two of the electrode/PEM interfaces leads to lower photocurrents. This clearly indicates that further work is needed for preparing a truly three-dimensional interface between the electrode and the PEM. This will require the development of methods for the effective penetration of the micelles through the pores of the photoelectrodes. Obviously, the use of a droplet of liquid electrolyte ensures that the internal surface of the nanoporous electrodes fully works from an electrochemical point of view.

Scheme 2. Schematic Diagram Showing the Configuration of the Different Tandem Cells Studied[a]

TANDEM	P:α-Fe_2O_3 (Photoanode)	INTERFACE	MEMBRANE FAA-3-20	INTERFACE	Fe:CuO (Photocathode)
1		0.1M KOH		0.1M KOH	
2		¼ FAA-3		0.1M KOH	
3		0.1M KOH		FAA-3	
4		¼ FAA-3		FAA-3	

[a]The additive employed for improving the electrode/PEM interface is indicated in each case together with the nomenclature/color used in the figures in this work.

The stability of the tandem cells studied was analyzed through chronoamperometric measurements for 1 h at an applied bias of 0.65 V. The results show (Figure 6a) that the tandem cell number 3, combining diluted KOH at the photoanode and a diluted ionomer at the photocathode for interface formation, is characterized by a remarkable stability. This could be linked to the fact that for this tandem cell, a droplet of the ionomer dispersion was placed at the junction between the Fe/CuO photocathode and the PEM, alleviating the intrinsic stability problems in such a way usually observed for this semiconductor material in liquid electrolytes. The

DOI: 10.1021/acsami.8b06826
ACS Appl. Mater. Interfaces 2018, 10, 25393−25400

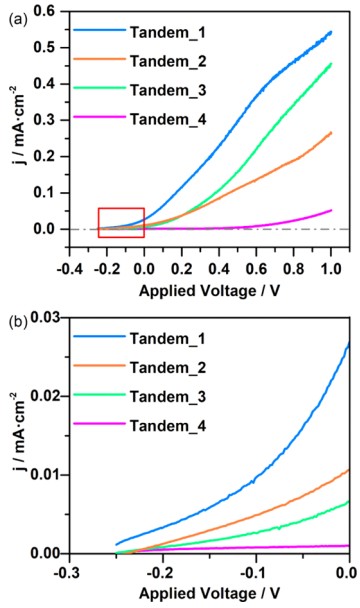

Figure 5. Current density−voltage curves obtained under standard illumination (AM 1.5G) for the different tandem cells. Panel (a) shows the curves with a cell voltage window ranging from −0.25 to 1 V and panel (b) shows a detail of the region marked with a rectangle in panel (a), the bias-free region. Cell voltage is defined as the difference of potential between the photoanode and the photocathode.

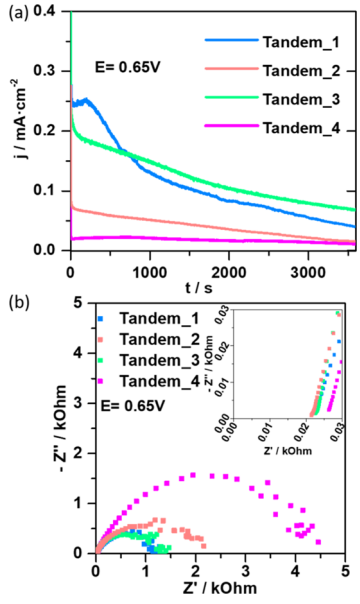

Figure 6. (a) Current density vs time curves and (b) Nyquist plots collected under standard illumination (AM 1.5G) at a fixed voltage of 0.65 V for the different tandem cells studied.

unsatisfactory results in terms of photocurrent obtained for cell 4 clearly indicate that it is necessary to improve the interface between the photoelectrodes and the membrane, especially in the case of hematite. The employment of an ionomer dispersion increases the stability of the device, particularly in the case of copper oxide compared with previously reported stabilities;[30] however, in the case of hematite, the employment of an ionomer dispersion leads to a dramatic decrease of the photoresponse. This behavior is probably related to the fact that the ionomer dispersion does not completely penetrate the mesoporous structure. The PEC results agree with the EIS shown in Figure 6b. The Nyquist plots were collected under illumination (AM 1.5G) for an applied bias of 0.65 V for the different tandem cells (see Scheme 2) to study the kinetics of charge-transfer processes under PEC operating conditions. The charge-transfer resistance at the semiconductor/electrolyte interface is associated with the radius of the semicircle in the frequency range 1−100 Hz. Figure 6b shows that the cell 4 (both interfaces formed by the ionomer dispersion) has a much larger impedance arc radius, indicating that the charge-transfer kinetics is hindered, which is likely linked to the fact that the interface electrode/PEM needs to be improved. Moreover, cell number 1 and 3 present the smallest impedance arc radius, indicating that the charge-transfer kinetics is much faster. This result agrees with the fact that in both cases (Tandem_1 and Tandem_3), the interface between the photoanode and the membrane includes a droplet of an aqueous KOH solution, which ensures the complete wetting of the inner electrode area.

Admittedly, at this development stage of the tandem cell design, it is not possible to quantify the amount of photogenerated H_2 and O_2. In fact, part of the photocurrent is thought to be associated with the photocorrosion of the electrode material (in the case of CuO-based electrodes). To assess the potential occurrence of photocorrosion and also to illustrate the advantage of using a PEM for increasing device stability, additional experiments were carried out to characterize the state of different Fe/CuO electrodes. Samples freshly prepared or submitted to equivalent PEC experiments in the tandem cell (TC electrodes) or in a conventional three-electrode cell with an aqueous 0.1 M KOH bulk liquid electrolyte (PC electrodes) were studied. The same charge (0.4 C) was passed through both TC and PC electrodes under standard illumination. UV−vis absorption measurements, Raman spectroscopy, and XPS analysis were carried out. The results are shown in Figures 7 and S3. For the TC electrodes, the absorbance slightly decreases compared to that of the as-prepared Fe/CuO electrodes, while retaining the same Raman fingerprint. In contrast, the Raman spectra for the PC electrodes show the appearance of a band at 209.5 cm^{-1}, corresponding to Cu_2O,[31] together with a substantial bleaching of the electrode. However, the XPS analysis confirms that the main oxidation state of copper is +2. In any case, a comparison between TC and PC electrodes clearly reveals the beneficial stabilization effect of the PEM tandem configuration.

On the other hand, the results shown in Figure S3 show no significant differences among P:α-Fe_2O_3 samples either freshly prepared or used in the tandem or conventional cell. This demonstrates that no significant photocorrosion occurs in the case of hematite regardless of the nature of the electrolyte.

CONCLUSIONS

In summary, the concept of a bias-free tandem cell based on a phosphorus-modified hematite photoanode and an iron-modified copper oxide photocathode for water splitting with the employment of an alkaline electrolyte membrane (Fumatech, FAA-3-20) has been demonstrated. However, it is also evident that photoresponse needs to be dramatically enhanced under bias-free operating conditions. It is important to highlight that the employment of a polymer membrane electrolyte instead of the typical acidic or basic bulk aqueous electrolyte diminishes the photocorrosion of the photo-

DOI: 10.1021/acsami.8b06826
ACS Appl. Mater. Interfaces 2018, 10, 25393−25400

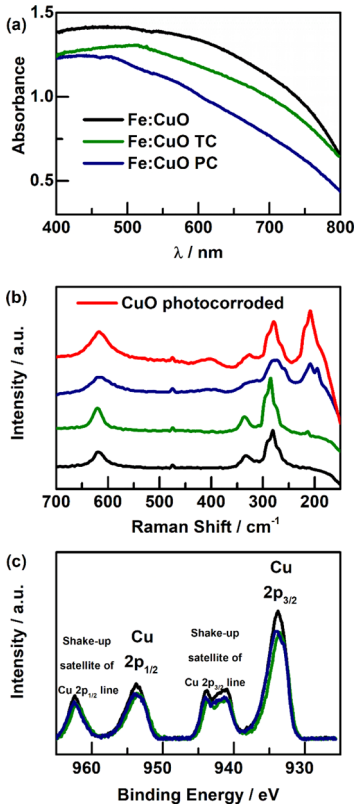

Figure 7. Characterization of Fe/CuO electrodes: freshly prepared (black), used in a tandem cell (TC, green) and used in a conventional three-electrode cell (PC, blue). (a) UV−vis spectra, (b) Raman spectra, and (c) Cu 2p XPS spectra. The same charge was passed through both TC and PC electrodes (0.4 C) with 1 sun illumination. Note that the red curve shown in panel (b) corresponds to a photocorroded iron-free cupric oxide electrode.

electrodes, increasing the stability of the device. This is illustrated in the case of the iron-modified copper oxide, for which the employment of the ionomer dispersion considerably increases the stability. However, work is still needed for improving the interface between the photoelectrode and the membrane. Furthermore, the employment of other electrodes with better photoresponse, the addition of cocatalysts, and using alternative PEMs are obvious ways forward under way in our laboratories.

EXPERIMENTAL DETAILS

All solutions were prepared with deionized water with a resistivity higher than 15 MΩ·cm^{-1}.

Synthesis of (110) Oriented Hematite Nanorods. The methodology employed to synthesize the (110) oriented hematite nanorods is based on the work of Vayssieres et al.[32] The synthesis consists of a chemical bath deposition procedure followed by a thermal treatment. It entails placing 100 mL of an aqueous solution containing 0.15 mol·L^{-1} ferric chloride ($FeCl_3·6H_2O$, Sigma-Aldrich, 99%) and 1 mol·L^{-1} sodium nitrate ($NaNO_3$, Sigma-Aldrich, 99%) into a regular stopped flask containing fluorine tin oxide (FTO) glass substrates supported vertically on the flask wall. The flask is heated in a regular stove at 100 °C for 6 h. Finally, a heat treatment in air at 600 °C for 1 h is required to obtain the hematite phase of ferric oxide, with a nanorod-based morphology.

Hematite Modification with Phosphorus. The modification of hematite electrodes with P is achieved by spraying a solution containing 0.1 mol·L^{-1} $(NH_4)_2HPO_4$ (Sigma-Aldrich, 99%) and isopropyl alcohol in a 1:10 ratio onto the hematite electrodes. The coated electrode is dried at 70 °C on a hot plate. Finally, the electrodes are thermally annealed at 450 °C for 30 min in air.

Synthesis of Copper Oxide. The synthesis comprises two steps and it is based on the works of Kang et al.[30] and Lin et al.[19] First, Cu films are electrodeposited from an aqueous solution containing 0.1 mol·L^{-1} copper nitrate ($Cu(NO_3)_2·3H_2O$, Labkem, analytical grade ACS) and 3 mol·L^{-1} lactic acid ($C_3H_6O_3$, Sigma-Aldrich, 85%, FCC) at a fixed pH value of 5, adjusted by adding sodium hydroxide pellets (NaOH, Scharlau, extrapure). The electrodeposition is performed at a constant potential of −0.3 V (vs Ag/AgCl) for 1 h. After electrodeposition, the electrodes are rinsed with deionized water and chemical oxidation is performed through their immersion in an aqueous solution containing 2.5 mol·L^{-1} sodium hydroxide (NaOH, Scharlau, extrapure) and 0.125 mol·L^{-1} ammonium persulfate [$(NH_4)_2S_2O_8$ Sigma-Aldrich, 98%] for 3 min. Finally, the electrodes are thermally treated in air at 450 °C for 1 h.

Copper Oxide Modification by Fe Addition through Drop-Casting. Once the copper oxide thin films were prepared, the Fe-precursor was added through an impregnation method (drop-casting).[26] The employed precursor was ferric chloride hexahydrate ($FeCl_3·6H_2O$, Sigma-Aldrich, 99%) in a concentration of 3.30×10^{-4} mol·L^{-1}. This procedure was repeated four times. Finally, a thermal treatment at 550 °C in air for 10 h was required.

Sample Characterization. The morphology of the different electrodes was studied by an FEI XL30 field-emission gun scanning electron microscope, operating at 25 kV.

The crystal structures of hematite and copper oxide were identified by XRD (Bruker D8-ADVANCE, using Cu Kα radiation) operating at 40 kV and 40 mA in the 2θ range from 20° to 70° in the case of hematite and from 30° to 80° in the case of copper oxide, both at a step scan of 1°·min^{-1}.

XPS was used for compositional analysis and for characterization of the iron, copper, and phosphorus oxidation states (K-Alpha Thermo-Scientific).

(Photo)electrochemical Characterization. The experimental device consists of a tandem cell formed by a photoanode based on hematite modified with phosphorus (P:α-Fe_2O_3) and a photocathode based on copper oxide modified with iron (Fe/CuO). The electrode−membrane interfaces are formed by adding a droplet of the ionomer dispersion obtained by dissolving FAA3 powder (5.7 wt %) in isopropanol or by using a droplet of the potassium hydroxide solution ($V_{droplet}$ = 15 μL). The hydrated alkaline membrane FAA3 had a thickness of 20 μm (Fumion Fumasep FAA-3-20 from Fumatech) and it is transparent to visible light. A silver paste was deposited over the uncoated edge of each FTO substrate to favor electrical contact with the current collectors. Different configurations have been tested, as shown in Scheme 1. In the case of the study of the cells formed by only one photoelectrode (Scheme 1a,b), the device was illuminated through the photoelectrode glass substrate, whereas in the case of the tandem cell formed by both photoelectrodes, the cell was illuminated through the photoanode glass substrate. The photoelectrode area exposed to illumination was 0.5 cm^2. A scanning potentiostat (Potentiostat/Galvanostat Metrohm AUTOLAB) equipped with a frequency response analyzer (FRA Metrohm AUTOLAB) was used to record linear sweep voltammograms in the dark and under illumination at a scan rate of 10 mV·s^{-1} and EIS in the range from 100 to 0.01 Hz. An Oriel solar simulator providing an irradiation of 100 mW·cm^{-2} (AM 1.5G) was used for illumination.

ASSOCIATED CONTENT

Supporting Information

The Supporting Information is available free of charge on the ACS Publications website at DOI: 10.1021/acsami.8b06826.

Additional experimental details; material characterization; and pictures of the real experimental device (PDF)

DOI: 10.1021/acsami.8b06826
ACS Appl. Mater. Interfaces 2018, 10, 25393−25400

AUTHOR INFORMATION

Corresponding Author

*E-mail: roberto.gomez@ua.es. Phone: +34 96 590 3748.

ORCID

Vincenzo Baglio: 0000-0002-0541-7169

Roberto Gómez: 0000-0002-5231-8032

Present Address

§Instituto de Carboquímica, CSIC, C/Miguel Luesma Castán 4, 50018 Zaragoza, Spain.

Funding

Authors gratefully acknowledge funding from the European Union's Horizon 2020 research and innovation programme under grant agreement no. 760930 (FotoH2 project).

Notes

The authors declare no competing financial interest.

ACKNOWLEDGMENTS

A.C. acknowledges the University of Alicante for a predoctoral grant (FPU-UA) and also thanks the Vicepresidency of Research, Development and Innovation of University of Alicante for a mobility grant. Authors are also grateful to Dr. Teresa Lana-Villarreal for the acquisition of Raman spectra.

REFERENCES

(1) Prévot, M. S.; Sivula, K. Photoelectrochemical Tandem Cells for Solar Water Splitting. *J. Phys. Chem. C* **2013**, *117*, 17879−17893.

(2) Bornoz, P.; Abdi, F. F.; Tilley, S. D.; Dam, B.; van de Krol, R.; Graetzel, M.; Sivula, K. A Bismuth Vanadate-Cuprous Oxide Tandem Cell for Overall Solar Water Splitting. *J. Phys. Chem. C* **2014**, *118*, 16959−16966.

(3) Gurudayal; Sabba, D.; Kumar, M. H.; Wong, L. H.; Barber, J.; Grätzel, M.; Mathews, N. Perovskite-Hematite Tandem Cells for Efficient Overall Solar Driven Water Splitting. *Nano Lett.* **2015**, *15*, 3833−3839.

(4) Kim, J. H.; Kaneko, H.; Minegishi, T.; Kubota, J.; Domen, K.; Lee, J. S. Overall Photoelectrochemical Water Splitting Using Tandem Cell under Simulated Sunlight. *ChemSusChem* **2016**, *9*, 61−66.

(5) Peter, L. M.; Upul Wijayantha, K. G. Photoelectrochemical Water Splitting at Semiconductor Electrodes: Fundamental Problems and New Perspectives. *ChemPhysChem* **2014**, *15*, 1983−1995.

(6) Siracusano, S.; Baglio, V.; Van Dijk, N.; Merlo, L.; Aricò, A. S. Enhanced performance and durability of low catalyst loading PEM water electrolyser based on a short-side chain perfluorosulfonic ionomer. *Appl. Energy* **2017**, *192*, 477−489.

(7) Aricò, A.; Girolamo, M.; Siracusano, S.; Sebastian, D.; Baglio, V.; Schuster, M. Polymer Electrolyte Membranes for Water Photo-Electrolysis. *Membranes* **2017**, *7*, 25.

(8) Sivula, K.; Le Formal, F.; Grätzel, M. Solar Water Splitting: Progress Using Hematite (α-Fe2O3) Photoelectrodes. *ChemSusChem* **2011**, *4*, 432−449.

(9) Gurudayal; Chiam, S. Y.; Kumar, M. H.; Bassi, P. S.; Seng, H. L.; Barber, J.; Wong, L. H. Improving the Efficiency of Hematite Nanorods for Photoelectrochemical Water Splitting by Doping with Manganese. *ACS Appl. Mater. Interfaces* **2014**, *6*, 5852−5859.

(10) Iordanova, N.; Dupuis, M.; Rosso, K. M. Charge transport in metal oxides: A theoretical study of hematite α-Fe2O3. *J. Chem. Phys.* **2005**, *122*, 144305−144310.

(11) Pendlebury, S. R.; Barroso, M.; Cowan, A. J.; Sivula, K.; Tang, J.; Grätzel, M.; Klug, D.; Durrant, J. R. Dynamics of photogenerated holes in nanocrystalline α-Fe2O3electrodes for water oxidation probed by transient absorption spectroscopy. *Chem. Commun.* **2011**, *47*, 716−718.

(12) Joly, A. G.; Williams, J. R.; Chambers, S. A.; Xiong, G.; Hess, W. P.; Laman, D. M. Carrier dynamics in Fe2O3 (0001) thin films and single crystals probed by femtosecond transient absorption and reflectivity. *J. Appl. Phys.* **2006**, *99*, 053521−053526.

(13) Shen, S.; Li, M.; Guo, L.; Jiang, J.; Mao, S. S. Surface Passivation of Undoped Hematite Nanorod Arrays via Aqueous Solution Growth for Improved Photoelectrochemical Water Splitting. *J. Colloid Interface Sci.* **2014**, *427*, 20−24.

(14) Ulman, K.; Nguyen, M.-T.; Seriani, N.; Gebauer, R. Passivation of surface states of α-Fe2O3(0001) surface by deposition of Ga2O3 overlayers: A density functional theory study. *J. Chem. Phys.* **2016**, *144*, 094701−094706.

(15) Hussain, S.; Hussain, S.; Waleed, A.; Tavakoli, M. M.; Wang, Z.; Yang, S.; Fan, Z.; Nadeem, M. A. Fabrication of CuFe2O4/α-Fe2O3 Composite Thin Films on FTO Coated Glass and 3-D Nanospike Structures for Efficient Photoelectrochemical Water Splitting. *ACS Appl. Mater. Interfaces* **2016**, *8*, 35315−35322.

(16) Cots, A.; Cibrev, D.; Bonete, P.; Gómez, R. Hematite Nanorod Electrodes Modified with Molybdenum: Photoelectrochemical Studies. *ChemElectroChem* **2017**, *4*, 585−593.

(17) Cots, A.; Gómez, R. Ytterbium Modification of Pristine and Molybdenum-Modified Hematite Electrodes as a Strategy for Efficient Water Splitting Photoanodes. *Appl. Catal., B* **2017**, *219*, 492−500.

(18) Zhang, Y.; Jiang, S.; Song, W.; Zhou, P.; Ji, H.; Ma, W.; Hao, W.; Chen, C.; Zhao, J. Nonmetal P-Doped Hematite Photoanode with Enhanced Electron Mobility and High Water Oxidation Activity. *Energy Environ. Sci.* **2015**, *8*, 1231−1236.

(19) Hsu, Y.-K.; Yu, C.-H.; Lin, H.-H.; Chen, Y.-C.; Lin, Y.-G. Template Synthesis of Copper Oxide Nanowires for Photo-electrochemical Hydrogen Generation. *J. Electroanal. Chem.* **2013**, *704*, 19−23.

(20) Kargar, A.; Jing, Y.; Kim, S. J.; Riley, C. T.; Pan, X.; Wang, D. ZnO/CuO Heterojunction Branched Nanowires for Photoelectro-chemical Hydrogen Generation. *ACS Nano* **2013**, *7*, 11112−11120.

(21) Oh, H. B.; Ryu, H.; Lee, W. J. Vertical Growth of Cupric Oxide Nanorods for Photoelectrode Using a Modified Chemical Bath Deposition Method. *J. Electrochem. Soc.* **2014**, *161*, H578−H582.

(22) Oh, H.-b.; Ryu, H.; Lee, W.-J. Effects of Copper Precursor Concentration on the Growth of Cupric Oxide Nanorods for Photoelectrode Using a Modified Chemical Bath Deposition Method. *J. Alloys Compd.* **2015**, *620*, 55−59.

(23) Guo, X.; Diao, P.; Xu, D.; Huang, S.; Yang, Y.; Jin, T. CuO/Pd Composite Photocathodes for Photoelectrochemical Hydrogen Evolution Reaction. *Int. J. Hydrogen Energy* **2014**, *39*, 7686−7696.

(24) Tripathi, M.; Chawla, P. Optimization of semiconductor ns-TiO2-CuO admixed photoelectrode for photoelectrochemical solar cell in regard to hydrogen production. *Int. J. Hydrogen Energy* **2016**, *41*, 7993−7996.

(25) Tang, H.; Matin, M. A.; Wang, H.; Sudhakar, S.; Chen, L.; Al-Jassim, M. M.; Yan, Y. Enhancing the Stability of CuO Thin-Film Photoelectrodes by Ti Alloying. *J. Electron. Mater.* **2012**, *41*, 3062−3067.

(26) Cots, A.; Bonete, P.; Gómez, R. Improving the Stability and Efficiency of CuO Photocathodes for Solar Hydrogen Production through Modification with Iron. *ACS Appl. Mater. Interfaces*, DOI: 10.1021/acsami.8b09892.

(27) Hu, Z.; Shen, Z.; Yu, J. C. Covalent Fixation of Surface Oxygen Atoms on Hematite Photoanode for Enhanced Water Oxidation. *Chem. Mater.* **2016**, *28*, 564−572.

(28) Xiong, D.; Li, W.; Wang, X.; Liu, L. Passivation of Hematite Nanorod Photoanodes with a Phosphorus Overlayer for Enhanced Photoelectrochemical Water Oxidation. *Nanotechnology* **2016**, *27*, 375401.

(29) Tahir, D.; Tougaard, S. Electronic and optical properties of Cu, CuO and Cu2O studied by electron spectroscopy. *J. Phys.: Condens. Matter* **2012**, *24*, 175002−175010.

(30) Zheng, J. Y.; Song, G.; Kim, C. W.; Kang, Y. S. Facile preparation of p-CuO and p-CuO/n-CuWO4 junction thin films and their photoelectrochemical properties. *Electrochim. Acta* **2012**, *69*, 340−344.

DOI: 10.1021/acsami.8b06826
ACS Appl. Mater. Interfaces 2018, 10, 25393−25400

(31) Gan, T.; Wang, Z.; Shi, Z.; Zheng, D.; Sun, J.; Liu, Y. Graphene oxide reinforced core-shell structured Ag@Cu 2 O with tunable hierarchical morphologies and their morphology-dependent electrocatalytic properties for bio-sensing applications. *Biosens. Bioelectron.* **2018**, *112*, 23−30.
(32) Vayssieres, L.; Beermann, N.; Lindquist, S.-E.; Hagfeldt, A. Controlled Aqueous Chemical Growth of Oriented Three-Dimensional Crystalline Nanorod Arrays: Application to iron(III) Oxides. *Chem. Mater.* **2001**, *13*, 233−235.

DOI: 10.1021/acsami.8b06826
ACS Appl. Mater. Interfaces 2018, 10, 25393−25400